

Reports

Influence of Land-Surface Evapotranspiration on the Earth's Climate

Abstract. Calculations with a numerical model of the atmosphere show that the global fields of rainfall, temperature, and motion strongly depend on the land-surface evapotranspiration. This confirms the long-held idea that the surface vegetation, which produces the evapotranspiration, is an important factor in the earth's climate.

That vegetation influences climate—and, especially, that the clearing of forests reduces rainfall—is an old idea. For example, the biography of Christopher Columbus by his son Ferdinand (1) states that “on Tuesday, July 22d [1494], he departed for Jamaica. . . . The sky, air, and climate were just the same as in other places; every afternoon there was a rain squall that lasted for about an hour. The admiral writes that he attributes this to the great forests of that land; he knew from experience that formerly this also occurred in the Canary, Madeira, and Azore Islands, but since the removal of forests that once covered those islands they do not have so much mist and rain as before.”

Averaged for the globe, and for the year, the measured river water drainage

from the continents is about one-third as large as the measured precipitation, which means that the average land-surface evapotranspiration is about two-thirds as large as the precipitation (2). In some regions, during some months of the year, the land-surface evapotranspiration is larger than the precipitation. For example, averaged over the central and eastern United States, in July, the precipitation is about 90 mm per month and the evapotranspiration is about 120 mm per month (3, 4). This is possible because of the moisture that was stored in the plant root zone of the soil during the preceding months of the year.

But the fact that the land-surface evapotranspiration, acting through the vegetation, sometimes exceeds the precipitation does not necessarily mean that

reducing or increasing the land-surface evapotranspiration will reduce or increase the precipitation. The connection between evapotranspiration and precipitation is difficult to ascertain because it depends on a large number of interacting thermodynamic and dynamical processes, which must be taken into account in a quantitative way.

Numerical models have been developed which quantitatively synthesize the many physical processes that produce the atmospheric general circulation and global climate, including the precipitation [for example, see (5)]. These models fairly successfully simulate the principal geographic and seasonal characteristics of the observed precipitation: the inter-tropical convergence rains over South America and Africa and their seasonal displacements; the summer monsoon rains over India and southeast Asia; the deserts in subtropical north and south Africa, North America, South America, Asia, and Australia; and, in the extratropics, the rainstorms and snowstorms of the wave cyclones in winter and the airmass convective rains of summer (6). By using one of these numerical models of the atmosphere and prescribing the land-surface evapotranspiration in a controlled sensitivity experiment, we can determine how this boundary condition influences the model-produced climate.

For the present experiment, the current version of the Goddard Laboratory for Atmospheric Sciences (GLAS) atmospheric general circulation model is used. Starting from a given initial state, the conservation equations for mass, momentum, moisture, and energy, expressed in finite-difference form for a spherical grid, are used to calculate the evolution of the pressure field at the earth's surface and of the fields of wind, temperature, and water vapor at nine levels between the surface and an elevation of 20 km. The fields of the convective clouds and precipitation and the large-scale upglide clouds and precipitation are also calculated, with a horizontal resolution of 4° of latitude and 5° of longitude over the globe and a nearly continuous variation in time. The prescribed surface boundary conditions are the ocean surface temperature, the large-scale topography and surface roughness, the surface albedo, and, in this experiment, the amount of moisture in the soil that is available for evapotranspiration. (In other applications the model soil moisture is a dependent variable, which varies with time according to the calculated precipitation and evapotranspiration.) Shukla *et al.* (7) have described the current GLAS model and evaluated its

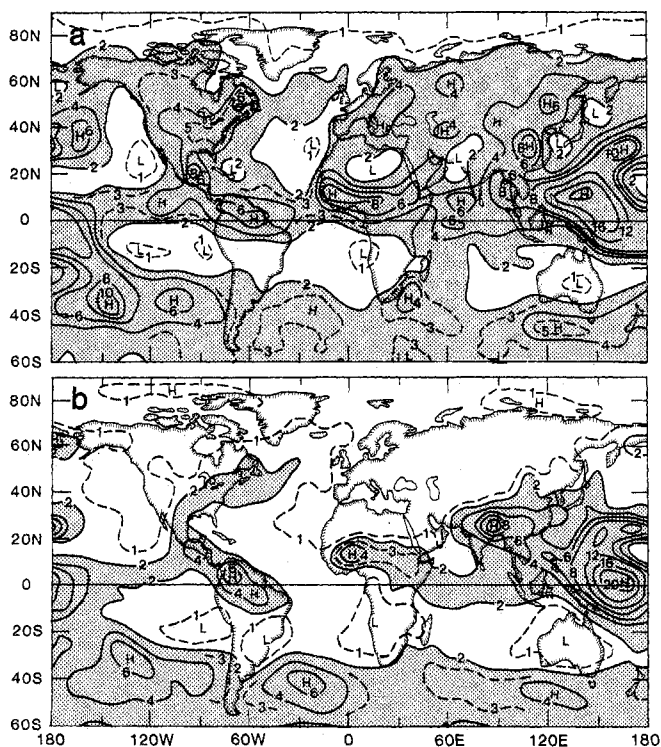


Fig. 1. Simulated July precipitation (millimeters per day) in (a) the wet-soil and (b) the dry-soil case.

ability to simulate the observed winter and summer season mean atmospheric fields and their intraseasonal variations.

We place two different constraints on the land-surface evapotranspiration: in one case the evapotranspiration is always set equal to the potential evapotranspiration calculated by the model (this is the evapotranspiration when the soil is moist and completely covered by vegetation); in the other case no evapotranspiration is allowed to take place. In principle, the first of these conditions would be physically realizable on an earth that is completely covered with vegetation and is irrigated where necessary, whereas the second would be approached on an earth that is completely and permanently devoid of vegetation. We refer to the calculations made with these two conditions as the wet-soil case and the dry-soil case.

Starting from an observed atmospheric state on 15 June, the integrations for the dry-soil and wet-soil cases were carried forward for 60 days. The results shown here are the time-averaged fields for July, the month when the Northern Hemisphere extratropics has the maximum potential evapotranspiration. An examination of the subsequent 15 days of integration, 1 to 15 August, showed that in both cases the July results had almost reached equilibrium with the prescribed boundary conditions.

Figure 1 shows the precipitation in the two cases. In the wet-soil case, the precipitation over Europe and over most of Asia is about 4 mm/day and does not differ much from the calculated potential evapotranspiration. But in the dry-soil case, Europe and most of Asia have almost no precipitation. Only over southeast Asia and India, in the dry-soil case, is there transport of water vapor from the ocean which produces heavy rain and in this case the precipitation in that region most closely resembles the observed summer rainfall.

Over most of North America the precipitation in the wet-soil case is between 3 and 6 mm/day, and for the most part it too is roughly equal to the local evapotranspiration. The exception is the southwest-northeast band of maximum rainfall across the eastern part of the continent, where there is a water vapor transport convergence of about 1 to 3 mm/day. But in the dry-soil case the precipitation over most of the continent is reduced to about 1 mm/day or less. Only the eastern part of the continent has a band of rainfall of about 2 mm/day, which consists of water transported from the ocean.

Over South America, the rainfall near

the equator in the wet-soil case is about 6 mm/day, which is about 2 mm/day larger than the evapotranspiration. In the dry-soil case the rainfall is almost as large, all of it being water transported from the ocean.

Across Africa, at about 10°N, the precipitation in the wet-soil case is about 4 mm/day larger than the local evapotranspiration, but north and south of the rain band the precipitation is about 2 to 3 mm/day smaller than the evapotranspiration; this means that there are substantial convergences and divergences in the water vapor transports. In the dry-soil case, there is a band of rain of 3 to 4 mm/day centered at about 14°N, and this precipitation is about the same as the amount by which the precipitation exceeded the evapotranspiration in the wet-soil case; this means that the convergence of the water vapor transport by the atmospheric circulation is about the same in the two cases.

Figure 2 shows the calculated land-surface temperature. North of about 20°S, the land-surface temperature is about 15° to 25°C warmer in the dry-soil case. There are two reasons for this: (i) there is no evaporative cooling of the land surface (which, in the wet-soil case, amounts to 125 W/m² when averaged between 20°S and 60°N) and (ii) there is a large increase in the heating of the ground by solar radiation (an increase from 172 to 258 W/m² when averaged between 20°S and 60°N). This is because the calculated cloudiness is less when

there is no land-surface evapotranspiration.

In the dry-soil case the net radiational heating of the land surface is balanced entirely by the conductive-convective transfer of sensible heat to the atmospheric planetary boundary layer, the lowest 1 to 2 km of the atmosphere. (This heat transfer to the atmosphere is 169 W/m² in the dry-soil case, compared to only 21 W/m² in the wet-soil case, when averaged for the land surface between 20°S and 60°N.) As a result, strong "thermal lows" develop over the land in the dry-soil case. Figure 3b shows these strong lows in the surface pressure reduced to sea level. The difference in the surface pressure, without reduction to sea level, is shown in Fig. 3c, and here we see the change in the geostrophic wind field at the earth's surface.

The decrease in surface pressure over the continents, about 5 to 15 mbar, is compensated by higher pressure over the oceans. But the pressure rise is not uniformly spread over the oceans. There is almost no change over the North Atlantic Ocean, and there is a large pressure rise over the mid-latitude North Pacific Ocean. The changes over the Northern Hemisphere continents and North Pacific Ocean greatly exceed the natural variability of the monthly mean July surface pressures that are produced by this general circulation model (the variability when the surface boundary conditions are held constant). In the extratropical South Atlantic and South Pacific, the

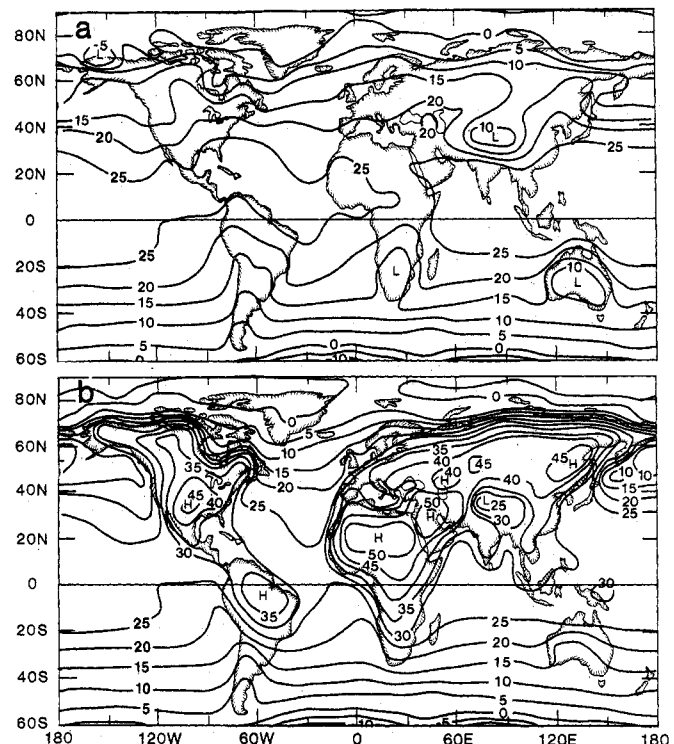


Fig. 2. Simulated July surface temperature (degrees Celsius) in (a) the wet-soil and (b) the dry-soil case.

differences in pressure between the two cases are just within the range of the natural variability of the monthly mean surface pressures produced by the model in those regions.

Examination of the vertical motion fields shows that in the dry-soil case there is an increased relative upward motion over the continents and sinking motion over the oceans. The accompanying low-level horizontal velocity convergence over the continents and divergence over the oceans generate and maintain the increased cyclonic vorticity over the continents and increased anticyclonic vorticity over the oceans. At the same time, the increased sinking motion over the oceans reduces the oceanic rainfall. But the increased rising motion over the continents does not increase the continental rainfall, because the land-surface evapotranspiration has been cut off.

There are three requirements for land-surface evapotranspiration: moisture in

the soil; vegetation, to transfer the moisture from the soil to the interface with the atmosphere; and energy, to convert that moisture (water) to water vapor. Most of the energy comes from radiational heating of the surface and therefore depends on surface albedo. In nature the albedo depends on the vegetation, which in turn depends on the soil moisture. But in numerical calculations we can make these factors independent of one another. Thus, in the present experiment, we let the soil moisture change but keep the albedo constant. Charney *et al.* (8) (in their cases 2a, 3a, and 4) keep the soil moisture constant but let the albedo change, and that too changes the evapotranspiration, precipitation, and circulation.

Vegetation and clouds play complementary roles: the clouds convert atmospheric water vapor into liquid water, which is transferred to the soil; the vegetation converts soil water into water vapor, which is transferred to the atmo-

sphere. In the extratropics, with its large seasonal changes, the soil plays a role analogous to that of the ocean. The ocean stores some of the radiational energy it receives in summer and uses it to heat the atmosphere over the ocean in winter. The soil stores some of the precipitation it receives in winter and uses it to humidify the atmosphere in summer.

If our calculations are indeed applicable to nature, the implication for forecasting extratropical summer rainfall is clear. In about the month of May the continental rainfall changes from the large-scale upglide condensation type to the cumulus convection type. If, after this change takes place, there is a large amount of moisture stored in the soil, the summer months that follow can have a large or small amount of rainfall, depending on the circulation conditions. But if the soil is dry, so that there is little or no evapotranspiration to keep the atmospheric planetary boundary layer moist, the remaining summer months will have little rainfall. Surface evapotranspiration, which requires moisture in the soil, is a necessary (though not sufficient) condition for extratropical summer precipitation. Observations of the soil moisture are therefore necessary for the precipitation predictions.

Finally, on the questions of whether the earth's vegetation cover and its modification by man have a significant influence on climate, and whether deforestation and afforestation, soil destruction and soil reclamation, or crop irrigation appreciably affect rainfall; the answer given by this study is that they do, if they are of large magnitude and large horizontal extent. But the exact response will vary from region to region, depending on how the large-scale circulation is modified.

J. SHUKLA

Laboratory for Atmospheric Sciences,
NASA/Goddard Space Flight Center,
Greenbelt, Maryland 20771

Y. MINTZ

Laboratory for Atmospheric Sciences,
NASA/Goddard Space Flight Center,
and Department of Meteorology,
University of Maryland,
College Park 20771

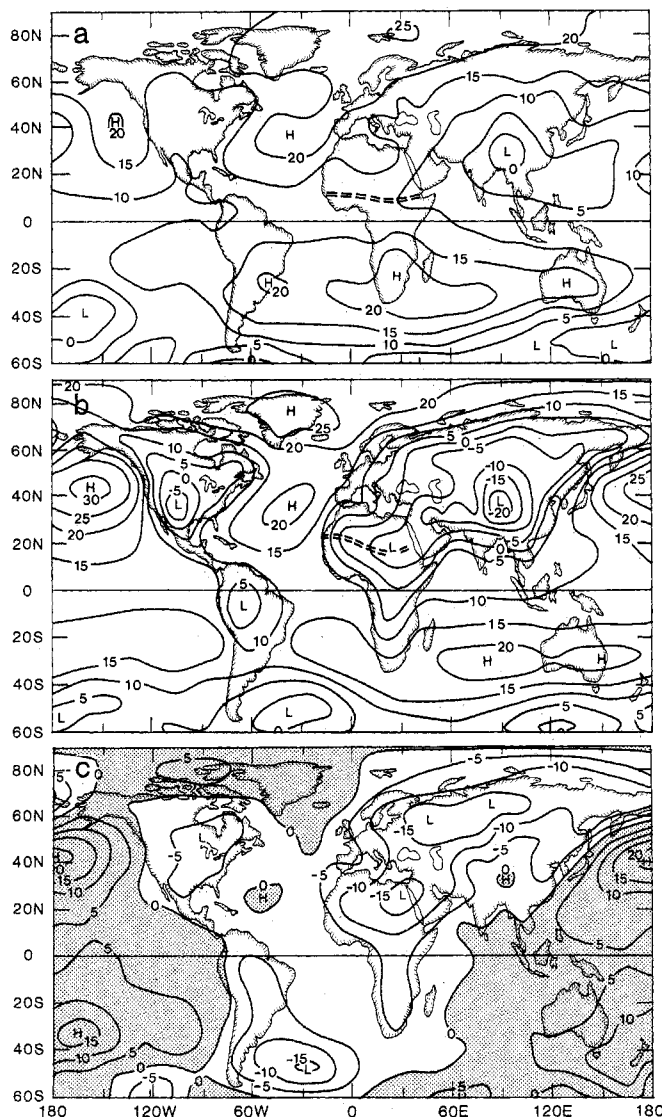


Fig. 3. Simulated July surface pressure reduced to sea level (millibars minus 1000) in (a) the wet-soil case and (b) the dry-soil case. (c) Difference between the surface pressure in the two cases.

References

1. F. Colon, *The Life of Christopher Columbus by His Son Ferdinand*, translated and annotated by B. Keen (Rutgers Univ. Press, New Brunswick, N.J., 1959), pp. 142-143.
2. H. Baumgartner and E. Reichel, *The World Water Balance: Mean Annual Global Continental and Maritime Precipitation, Evaporation and Runoff* (Elsevier, Amsterdam, 1975).
3. J. R. Mather, *Publ. Climatol.* 17, 3 (1964).
4. E. M. Rasmusson, *Mon. Weather Rev.* 96, 720 (1968).
5. J. Chang, Ed. *Methods in Computational Physics*, vol. 17, *General Circulation Models of the*

Atmosphere (Academic Press, New York, 1977).

6. WMO/ICSU, *Report of the Joint Organizing Committee Study Conference on Climate Models: Performance, Intercomparison and Sensitivity Studies* [GARP (Global Atmospheric Research Program) Publication Series 22, World Meteorological Organization, Geneva, 1979], vol. 1.

7. J. Shukla, D. Randall, D. Straus, Y. Sud, L. Marx, *Winter and Summer Simulations with the GLAS Climate Model* (National Aeronautics and Space Administration/Goddard Space Flight Center, Greenbelt, Md., in press).
8. J. Charney, W. J. Quirk, S. H. Chow, J. Kornfeld, *J. Atmos. Sci.* 34, 1366 (1977).

2 December 1981

Mass Extinctions in the Marine Fossil Record

Abstract. A new compilation of fossil data on invertebrate and vertebrate families indicates that four mass extinctions in the marine realm are statistically distinct from background extinction levels. These four occurred late in the Ordovician, Permian, Triassic, and Cretaceous periods. A fifth extinction event in the Devonian stands out from the background but is not statistically significant in these data. Background extinction rates appear to have declined since Cambrian time, which is consistent with the prediction that optimization of fitness should increase through evolutionary time.

A number of mass extinctions have "reset" major parts of the evolutionary system during the Phanerozoic. However, the precise timing and magnitude of these events has been difficult to measure because data from the fossil record are fragmentary. Comprehensive and accurate data on extinct species have always been unobtainable, and therefore most workers have been forced to investigate extinctions at the level of genera, families, and orders, with family-level data generally preferred as the best compromise between sampling limitations and taxonomic uncertainty (1). Historically, the three best summaries of familial data from the fossil record have been those of Newell (2), Cutbill and Funnell (3), and Valentine (4). But even with these data sets, identification of specific mass extinctions has been difficult and often subjective because of taxonomic problems and especially stratigraphic imprecision. Many macroevolutionary phenomena including mass extinctions have characteristic time scales that are geologically rather short (less than several tens of millions years) and can become lost or grossly distorted when analyzed without adequate stratigraphic control.

We now present a new analysis of extinctions based on a more comprehensive and accurate data set for marine animal families. Marine vertebrates as well as invertebrates and protozoans are included, and the data benefit from compilation of taxonomic and stratigraphic investigations far beyond traditional sources (5). The compilation encompasses approximately 3300 fossil marine families, of which about 2400 are extinct. Times of extinction for 87 percent of the families have been resolved to the level of the stratigraphic stage (mean duration, 7.4×10^6 years), and most of the remaining data has been resolved to strati-

graphic series (mean duration, 20×10^6 years).

The rates of extinction calculated from the familial data plotted against geologic time are illustrated in Fig. 1. Each point was calculated as follows: the number of families that became extinct in each of the 76 post-Tommotian (early Lower Cambrian) stages (6) was divided by the estimated duration of the stage (7); these initial rates were then modified by adding extinction rates calculated from the lower resolution series-level data to the appropriate stages. Calculations were made separately for "shelly" taxa and for rarely preserved taxa (8). The effect of this segregation was negligible in most cases so that the data for rarely preserved animals are not included with most points in Fig. 1. For four stages, however, addition of rarely preserved families increased calculated extinction rates by more than 0.5 family per million

years. These are the stages that contain the four major Lagerstätten of the Phanerozoic marine record: Burgess Shale (Cambrian, Templetonian), Hunsrück Shale (Devonian, Siegenian), Mazon Creek concretions (Carboniferous, Moscovian), and Solnhofen Limestone (Jurassic, "Tithonian"). The combined rates for shelly and rarely preserved families for these four stages are indicated in Fig. 1 by X's with the rates for shelly families shown below. Only the Burgess Shale (Templetonian) stands out on the plot.

The distribution of the 76 points for shelly animals in Fig. 1 suggests that two rates of extinction have been operative through the Phanerozoic. (i) Normal, or background, extinction: the majority of points fall in a rather tight cluster at extinction rates less than 8.0 extinctions per million years. (ii) Mass extinction: several points stand out as being considerably higher than the background and show a maximum of 19.3 familial extinctions per million years.

The problem of determining rigorously which points in Fig. 1 should be considered mass extinctions can be approached as a simple data analysis problem of identifying trends and outliers. As an initial step, we computed a linear regression (not shown) for all 76 extinction points as a function of geologic time and then searched for significant departures from this line. Four points (or 5 percent of the data) fell above the one-sided 99 percent confidence interval. These points, which are circled in Fig. 1, are (per million years) the Ashgillian (19.3 fm), Guadalupian (14.0 fm), Dzhulfian (15.7 fm), and Maestrichtian (16.3 fm). A fifth point, the Norian (10.8 fm), fell

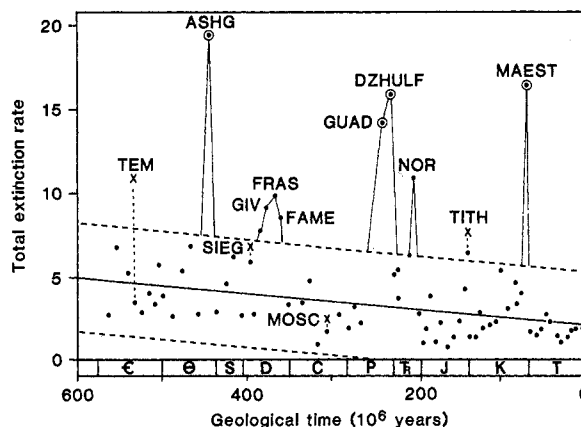


Fig. 1. Total extinction rate (extinctions per million years) through time for families of marine invertebrates and vertebrates. The plot shows statistically significant mass extinctions late in the Ordovician (ASHG), Permian (GUAD-DZHULF), Triassic (NOR), and Cretaceous (MAEST). An extinction event in the late Devonian (GIV-FRAS-FAME) is noticeable but not statistically significant. Circled points are those where the departure from the main cluster is highly significant ($P < .01$); X's indicate those cases where inclusion

of rarely preserved animal groups substantially increases the calculated extinction rate (the point directly below the X is the rate calculated without the rarely preserved groups). The figure also shows a general decline in background extinction rate through time. The regression line is fit to the 67 points having extinction rates less than eight families per 10^6 years, and the dashed lines define the 95 percent confidence band for the regression. Abbreviations: TEM, Templetonian; ASHG, Ashgillian; SIEG, Siegenian; GIV, Givetian; FRAS, Frasnian; FAME, Famennian; MOSC, Moscovian; GUAD, Guadalupian; DZHULF, Dzhulfian; NOR, Norian; TITH, Tithonian; MAEST, Maestrichtian.